Sveučilište u Rijeci
University of Rijeka
https://www.uniri.hr

Polytechnica: Journal of Technology Education, Volume 10, Number 1 (2026)
Politehnika: Časopis za tehnički odgoj i obrazovanje, Svezak 10, Broj 1 (2026)

Politehnika
Polytechnica
https://politehnika.uniri.hr
e-mail: cte@uniri.hr

DOI: https://doi.org/10.36978/cte.10.1.2

Stručni članak
Professional paper

Aerodynamic simulation and manufacturing of a carbon fiber-reinforced polymer spoiler for high-performance racing applications

Marin Krušvar
Department of Polytechnics
University of Rijeka
Sveučilišna avenija 4, 51000 Rijeka, Croatia
marin.krusvar@student.uniri.hr

Mateja Šnajdar
Department of Polytechnics
Dr. Franjo Tuđman Defense and Security University (SOIS FT)
Ilica 256 b, 10000 Zagreb, Croatia
mateja.snajdar@sois-ft.hr

Abstract

Presented paper explores the research and application of advanced materials, specifically carbon fiber-reinforced composites, in the automotive industry, with a particular focus on their use in the production of racing car parts. The application of carbon fiber-reinforced polymer (CFRP) composites in the design and production of racing car aerodynamic components, with emphasis on the development of a front spoiler. The study combines aerodynamic simulations, testing and manufacturing procedures, including mold fabrication and vacuum resin infusion, to produce a functional CFRP component intended to improve vehicle aerodynamic performance and stability. The proposed approach integrates computational fluid dynamics (CFD) based optimization with composite manufacturing techniques suitable for motorsport applications. By utilizing advanced computer simulations, testing and manufacturing techniques, such as resin vacuum infusion and mold fabrication, a functional vehide component that contributes to improving the aerodynamic properties and overall performance of the race car on the track was manufactured.

Keywords: *carbon-fiber composite; racing car; spoiler; resin; simulation*

1 Introduction

The continuous search for better performance in motor racing has spurred technological innovation in automobile technology, especially to produce light, resilient, and high-performance materials (Ahmad et al., 2020; Savage, 2008; Coşkun et al., 2025; Gilchrist and Curley, 1999). CFRP composites have attracted significant attention due to their excellent mechanical and lightweight properties. Such products have shown to have an extremely high strength-to-weight ratio, corrosion resistance, and better-than-average mechanical properties, which make them extremely suitable for use in situations where performance as well as lightness are desirable (Ozkan, Gok and Karaoglanli, 2020; Deakin and Crolla, 2000). In motorsport, where every gram of weight and every aerodynamic benefit can mean the difference between winning and losing (Deakin and Crolla, 2000), CFRPare now at the heart of racing-car construction. Among all the components of a race car that benefit from the use of carbon-fiber composites, aerodynamic elements such as spoilers come in at the head of improving vehicle stability, downforce, and overall handling. A racing car spoiler design should consider not just the material's properties but also its aerodynamic effectiveness. An ideally made spoiler can give a huge performance boost to the vehicle on the racetrack by optimizing grip and minimizing drag, giving the vehicle a beneficial boost (Rehkopf, 2011; Roslan et al., 2023; Ma, 2024). The presented paper describes the design, production, and testing of a carbon-fiber composite race car front spoiler with

emphasis on the application of advanced manufacturing technology in motor sport. The main intent of the study is to discuss the application of CFRP in producing the best aerodynamic component that has lightness combined with structural performance and optimal aerodynamic response. The process included the choice of suitable materials, application of sophisticated manufacturing techniques like resin vacuum infusion, and aerodynamic modelling to obtain the best design. The product was tested to assess the real-life performance. Based on the integration of theory and practice, in this paper it will be illustrated how new materials and new process technologies can be employed to produce high-performance components for cars to facilitate the overall competitiveness of racing cars. The outcome of this research not only will present some information on the application of CFRPin motorsport but also will act as a reference manual for further research and development in automotive engineering.

2 Materials and methods

2.1 Airfoil type

The choice of aerofoil was made according to the outcome of the 2D aerofoil table (Table 1), which was used when designing RITEH Racing Team RRC5 car. Aerofoils were chosen according to the biggest ratio between drag coefficient Cd and lift coefficient Cl at an angle of attack of 0° and the biggest ratio at an angle of attack between 10° and 15° (Airfoil Tools, 2025). The chosen aerofoils included: Eppler 664, Ch10sm, S1223, and MSHD. Coordinate files of the selected aerofoils were obtained from the Airfoil Tools database (Airfoil Tools, 2025). On the Airfoil Tools website, the suitable airfoil was chosen, with specified chord thickness and length and the coordinates of the chosen airfoil were downloaded. Since the dimensions of the spoiler was limited in height and length, coordinate files were downloaded with wing chord length varying from 50 mm to 400 mm in step sizes of 25 mm to create the desired configurations with ease.

Aerofoil	C_l	C_d	C_m	C_l/C_d
EPPLER 664	1.6795	0.0138	-0.4171	121.7911
ch10sm	1.2318	0.0108	-0.2799	114.5860
Fx 63-137	0.9315	0.0085	-0.2114	109.4595
a18	0.5998	0.0056	-0.1198	106.3475
e63	0.7546	0.0072	-0.1902	104.5152
s4022	0.7002	0.0069	-0.1694	101.6255
E423	1.1375	0.0114	-0.2441	99.5188
e423	1.1375	0.0115	-0.2441	98.9991
fx 74-c15	1.2011	0.0132	-0.252	91.0614
s1223	1.2073	0.0133	-0.2754	90.8427
sa7024	0.4191	0.0048	-0.0923	87.8616
davissm	0.7117	0.0089	-0.164	79.6085
a18sm	0.5044	0.0063	-0.1218	79.5584
e210	0.5607	0.0083	-0.1279	67.8814
GOE 531	1.2960	0.0194	-0.2972	66.7353
apex 16	0.4122	0.0068	-0.0975	60.3514
hq2090sm	0.2776	0.0058	-0.0609	47.6976
s7012	0.2692	0.0058	-0.0571	46.3339

Table 1. Results of 2D airfoil simulations at an angle of attack of 0° (Airfoil Tools, 2025)

2.2 Spoiler geometry

The geometry of the proposed front spoiler consists of 9 elements: the main wing, 4 flaps, 2 endplates, and 2 middle plates, Figure1 (Krušvar, 2024).

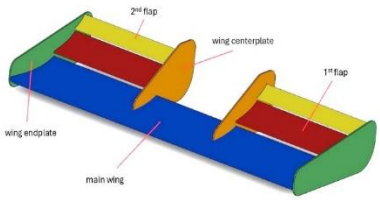

Figure 1. First version of front spoiler geometry (Krušvar, 2024)

The geometry was designed using SolidWorks software. The coordinate files were first prepared for work in SolidWorks and then imported to create the profile curve. All spoiler elements were constructed individually and then assembled into the front spoiler. Table 2 shows details of the six different spoiler configurations considered in the research (Krušvar, 2024). For each configuration, the aerofoils used for the main wing and two flaps, chord lengths and total angle of attack are specified. Data provided in Table 3 serves as an overview of the basic characteristics and differences between the tested configurations.

	configuration	spoiler profile	front spoiler with selected profile
1	main wing: Ch10sm 1st flap: Ch10sm 2nd flap: Ch10sm		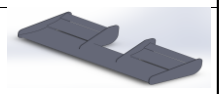
2	main wing: S1223 1st flap: S1223 2nd flap: S1223		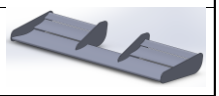
3	main wing: Eppler 664 1st flap: ch10sm 2nd flap: 1223		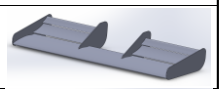
4	main wing: Eppler 664 1st flap: 1223 2nd flap: ch10sm		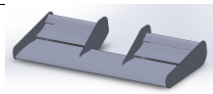
5	main wing: Eppler 664 1st flap: Ch10sm 2nd flap: MSHD		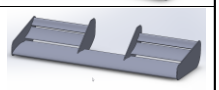
6	main wing: Eppler 664 1st flap: s1223 2nd flap: MSHD		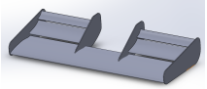
7	main wing: Eppler 664 1st flap: MSHD 2nd flap: 1223	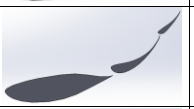	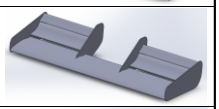
8	main wing: FX63137 1st flap: s1223 2nd flap: MSHD		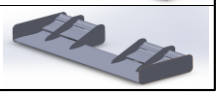

Table 2. Tested aerofoil configurations (Krušvar, 2024)

main wing aerofoil	first flap aerofoil	second flap aerofoil	chord lengths, mm	total angle of attack, °
Ch10sm	Ch10sm	Ch10sm	300, 150, 75	15.5
S1223	S1223	S1223	300, 150, 75	16
Eppler 664	Ch10sm	S1223	300, 150, 75	18
Eppler 664	S1223	Ch10sm	300, 150, 75	18
Eppler 664	Ch10sm	MSHD	300, 150, 75	18
Eppler 664	S1223	MSHD	300, 150, 75	18

Table 3. Overview of spoiler configurations with corresponding aerofoils, chord lengths, and total angles of attack

2.3 CFD methodology and simulation setup

Computational Fluid Dynamics (CFD) simulations were performed using the SimScale cloud-based Computer-Aided Engineering (CAE) platform, which supports aerodynamic, thermal and structural analyses. The use of cloud computing enabled a larger number of simulations and design iterations compared to conventional locally executed CAE software. Initially, aerodynamic analyses were conducted in open airflow conditions while the race car geometry was still under development. After all aerodynamically relevant components had been designed, the front spoiler was integrated into the complete vehicle model and simulations were performed on the entire race car assembly. The computational domain surrounding the spoiler and the complete vehicle represented a virtual wind tunnel.

The simulations were performed using the incompressible flow solver, assuming steady-state airflow conditions. Due to the geometrical symmetry of the race car and front spoiler, only half of the geometry was modelled in order to reduce computational time and resource requirements. Turbulence effects were modelled using the k–ω turbulence model, coupled with Reynolds-Averaged Navier–Stokes (RANS) equations. The k–ω model was selected because of its ability to accurately predict near-wall flow behaviour and flow separation phenomena relevant to aerodynamic components.

The simulation setup included definition of geometry, numerical mesh, fluid properties, initial conditions, boundary conditions, solver settings and result controls. Mesh generation consisted of both global and local mesh refinements, with increased mesh density around the vehicle surfaces and aerodynamic components to improve solution accuracy and capture local flow effects.

Air was selected as the working fluid, while density and kinematic viscosity values corresponded to standard atmospheric conditions. Default initial conditions provided by the solver were retained for all simulations to ensure consistency between investigated configurations.

Boundary conditions were applied as follows:

- Velocity inlet condition at the inlet surface with a constant airflow velocity of 20 m/s;
- Pressure outlet condition at the outlet surface with outlet pressure fixed at 0 Pa;
- Symmetry boundary condition applied on the symmetry plane to reduce computational cost;
- Slip wall condition applied to wind tunnel walls to neglect wall friction effects;
- Moving wall condition applied to the ground plane with velocity equal to inlet velocity, reproducing relative motion between the vehicle and ground;
- No-slip wall condition applied to all vehicle surfaces excluding wheels and axles to account for friction effects between air and the vehicle body;
- Rotating wall condition applied to wheels, including specification of rotation axis, rotation centre and angular velocity.

Simulation control parameters included time step settings, total simulation duration, iteration write

intervals, processor allocation and maximum simulation time. Identical solver settings were used for all investigated configurations to ensure result comparability.

The aerodynamic evaluation focused on lift (downforce) forces, drag forces, pressure distribution and velocity fields acting on individual spoiler elements, the complete front wing assembly and subsequently the entire vehicle. Streamline analysis was additionally used to evaluate flow separation between upper and lower aerofoil surfaces and to identify vortex formation downstream of the spoiler.

2.4 Aerodynamic coefficients and performance indicators

The aerodynamic behaviour of the investigated spoiler configurations was evaluated using aerodynamic coefficients Cl, Cd, and Cm, together with the corresponding aerodynamic forces and performance ratios obtained from CFD simulations.
The lift coefficient (Cl) represents the capability of an aerodynamic element to generate lift force. In racing vehicle applications, lift acts in the downward direction and therefore corresponds to downforce, improving tire grip, cornering ability, and vehicle stability at high speeds. Higher absolute values of Cl indicate stronger aerodynamic loading on the vehicle. The drag coefficient (Cd) describes aerodynamic resistance generated by the spoiler and vehicle geometry. Lower Cd values are preferred because excessive drag negatively influences vehicle acceleration and maximum speed. The moment coefficient (Cm) represents the aerodynamic pitching moment generated around a reference point and provides information regarding the influence of aerodynamic components on vehicle stability and load distribution. In the present study, the term lift (L) refers to the magnitude of the aerodynamic force generated by the spoiler. Since the investigated component is a front racing spoiler, the aerodynamic force acts downward and therefore represents downforce (negative lift) according to conventional aerodynamic sign conventions. For clarity and easier comparison between configurations, the obtained CFD results are presented as positive magnitudes of aerodynamic loading. Consequently, all positive lift values reported in Tables 5–7 correspond to generated downforce forces acting on the spoiler and vehicle. Although CFD post-processing in this study primarily reports lift force (L), drag force (D) and their ratio (L/D), these quantities directly correspond to the aerodynamic coefficients Cl and Cd, since lift and drag coefficients represent normalized forms of aerodynamic forces. Therefore, higher lift values indicate increased downforce generation, while lower drag values correspond to improved aerodynamic efficiency. The L/D ratio was used as the main performance indicator in the present work because it enables direct comparison between configurations by evaluating the ability to generate downforce relative to aerodynamic resistance. Higher L/D values indicate a more efficient spoiler configuration capable of producing greater aerodynamic loading with lower drag penalties.

In the investigated configurations, the highest lift values were achieved for Configuration 2, whereas Configuration 3 exhibited the highest aerodynamic efficiency due to its favourable lift-to-drag ratio. Final optimization of Configuration 7 focused on improving overall aerodynamic balance and airflow quality around the complete vehicle.

3 Results

3.1 Configuration development and influence of design modifications

Identical settings were applied in all simulations to ensure consistency. Aerodynamic performance was evaluated using lift (L), drag (D), and L/D ratio values derived from aerodynamic coefficients described in Section 2.4. Pressure and velocity fields were also examined. To assess the spoiler's aerodynamic behaviour, streamlines were used. The aim was to determine if flow separation happened between the aerofoil's upper and lower surfaces and to observe airflow behaviour downstream of the spoiler, including possible vortex formation (Figure 2).

The investigated configurations represent sequential design iterations aimed at improving aerodynamic performance by modifying the aerofoil combinations and local spoiler geometry. The parameters varied between configurations included the main wing aerofoil, first and second flap aerofoils, local flap geometry, and relative element positioning. The overview of tested combinations is given in Table 3, while the corresponding aerodynamic characteristics are summarized in Tables 4–6.

Configuration 1 used the Ch10sm aerofoil on all elements and served as the reference geometry. This configuration generated a total lift force of 183.6 N and drag of 27.97 N (L/D = 6.56). However, analysis showed only moderate aerodynamic behaviour compared with the remaining concepts and therefore the Ch10sm profile was retained only for flap applications in later iterations.

Configuration 2 replaced all elements with the S1223 profile, increasing lift from 183.6 N to 213.8 N, which represented the highest downforce among all tested spoiler concepts. Nevertheless, streamline analysis revealed flow separation on the second flap,

making the design impractical despite its favourable aerodynamic forces. To eliminate flow separation, two modified variants were developed. Configuration 2 mod 1 introduced trimming of the first flap tip, while Configuration 2 mod 2 increased the spacing between the flaps. These changes reduced aerodynamic loading, decreasing lift to 194.75 N and 196.55 N, respectively, while simultaneously improving flow stability and eliminating separation effects.

Configurations 3–7 investigated combinations based mainly on the Eppler 664 main wing profile with varying flap aerofoils. Configuration 3 (Eppler 664 + Ch10sm + S1223) produced the best aerodynamic efficiency among the baseline concepts, reaching the highest lift-to-drag ratio of 17.07 for the main wing. Configuration 7, consisting of Eppler 664 main wing, MSHD first flap and S1223 second flap, was selected for full-car simulations because it provided the most balanced aerodynamic behaviour and favourable flow characteristics. Additional optimization included installation of a plate parallel to the inner tire surface to direct airflow toward the diffuser. Five additional variants (7 mod 1–7 mod 5) were analysed by modifying element positions and relative angles.

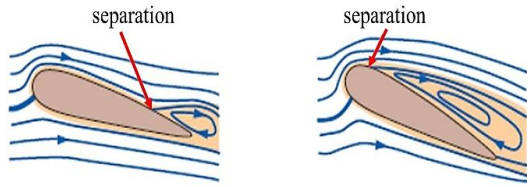

Figure 2. Separation of the air flow between the upper and lower surfaces of the profile (Krušvar, 2024)

Config.	Lift, *L*	Drag, *D*	*L/D*
1	183.60	27.97	6.56
1 car	75.00	24.12	3.10
2	213.80	32.54	6.57
2 mod 1	194.75	30.03	6.49
2 mod 2	196.55	31.33	6.27
3	169.06	64.99	2.60
4	180.46	29.89	6.04
5	188.94	31.63	5.97
6	189.75	32.30	5.87
7	190.14	32.96	5.77
7 mod 1	134.43	22.64	5.94
7 mod 2	132.83	19.78	6.72
7 mod 3	137.12	24.46	5.61
7 mod 4	137.22	21.21	6.47
7 mod 5	139.08	21.80	6.38
8	183.54	33.09	5.55

Table 4. Obtained simulation values of lift and drag for entire race car (Krušvar, 2024)

Config.	Lift, *L*	Drag, *D*	*L/D*
1	149.46	10.06	14.86
1 car	52.93	12.83	4.13
2	173.93	10.44	16.66
2 mod 1	165.28	11.80	14.01
2 mod 2	166.65	11.80	14.12
3	133.33	7.81	17.07
4	141.99	8.49	16.72
5	147.54	9.86	14.96
6	146.24	10.12	14.45
7	148.00	10.23	14.47
7 mod 1	108.77	6.20	17.54
7 mod 2	107.86	6.16	17.51
7 mod 3	109.96	6.29	17.48
7 mod 4	110.47	6.43	17.18
7 mod 5	110.80	6.31	17.56
8	144.30	9.42	15.32

Table 5. Obtained simulation values of lift and drag for main wing (Krušvar, 2024)

Config.	flap 1			flap 2		
	lift, *L*	drag, *D*	*L/D*	lift, *L*	drag, *D*	*L/D*
1	26.15	11.30	2.31	8.00	6.6	1.21
1 car	16.06	6.19	2.59	5.67	4.6	1.23
2	31.41	14.48	2.17	8.39	7.58	1.11
2 mod 1	20.48	10.68	1.92	8.99	7.54	1.19
2 mod 2	24.05	13.26	1.81	5.85	6.27	0.93
3	27.07	11.04	2.45	9.93	6.43	1.54
4	30.82	14.25	2.16	7.65	7.14	1.07
5	33.48	14.64	2.29	7.91	7.12	1.11
6	34.73	14.73	2.36	8.78	7.8	1.13
7	33.76	14.76	2.29	8.38	7.96	1.05
7 mod 1	20.79	8.24	2.52	3.89	4.66	0.83
7 mod 2	20.50	8.50	2.41	3.54	4.32	0.82
7 mod 3	21.85	8.52	2.56	4.23	4.85	0.87
7 mod 4	20.79	8.45	2.46	4.96	5.7	0.87
7 mod 5	21.61	8.51	2.54	5.64	6.15	0.92
8	35.23	19.1	1.84	3.94	4.56	0.86

Table 6. Obtained simulation values of lift and drag for flap 1 and flap 2 (Krušvar, 2024)

3.1.1 Configuration 1 simulation results

Given that the simulation results showed the Ch10sm profile provides only moderate performance compared to the other profiles, it was decided to limit its use to the flaps in later tests. Figure 3 shows the downforce values achieved, while Figure 4 illustrates the airflow pattern for this configuration.

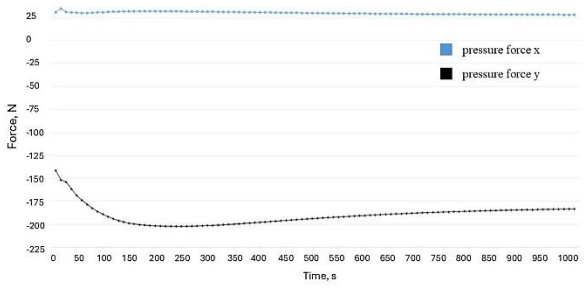

Figure 3. Obtained values of downforce for configuration 1 (Krušvar, 2024)

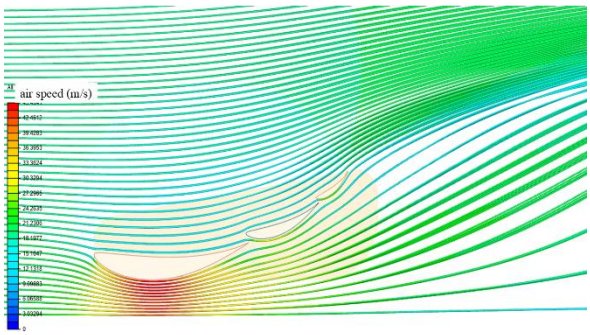

Figure 4. Airflow profile for configuration 1 (Krušvar, 2024)

3.1.2 Configuration 2

Flow separation was found on the second flap. Two design modifications were introduced to eliminate this issue: trimming the tip of the first flap and increasing the gap between the flaps (Figures 5-6). While this spoiler design produced the highest aerodynamic forces of all the tested options, it was still considered unsuitable for practical use.

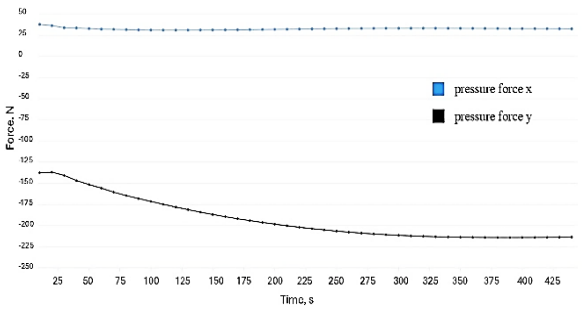

Figure 5. Obtained values of downforce for configuration 2 (Krušvar, 2024)

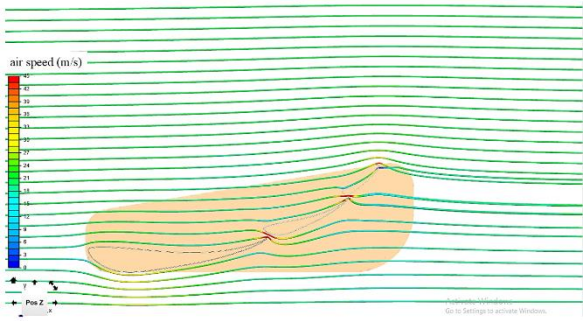

Figure 6. Airflow profile for configuration 2 (Krušvar, 2024)

3.1.3 Configuration 2 Mod 1

Simulation results confirmed that the separation issue had been resolved, making the spoiler usable. While there was a reduction in dynamic lift and drag forces, its performance was still better than that of the alternative profiles. A comparison between the two improved versions shows that the first outperforms the second. The second version displayed vortex formation behind the spoiler and a noticeable drop in velocity in that area, Figures 7-8.

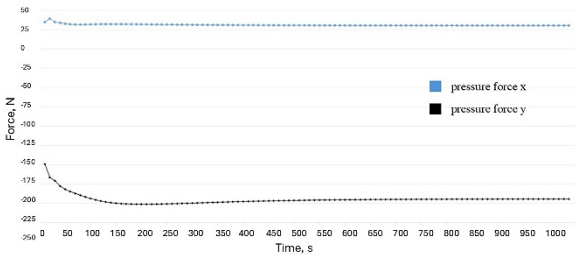

Figure 7. Obtained values of downforce for configuration 2 mod 1 (Krušvar, 2024)

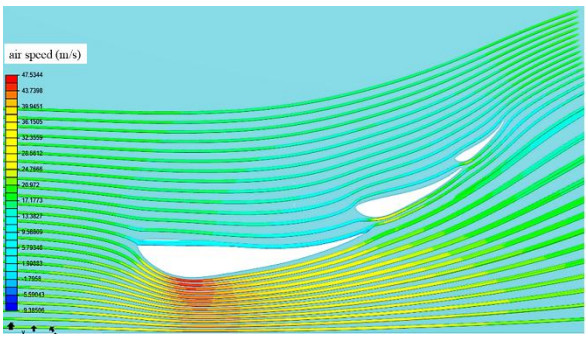

Figure 8. Airflow profile for configuration 2 mod 1 (Krušvar, 2024)

3.1.4 Configuration 3

Configuration 3 showed that the Eppler 664 aerofoil gives the best ratio of dynamic lift force to drag force, Figure 9.

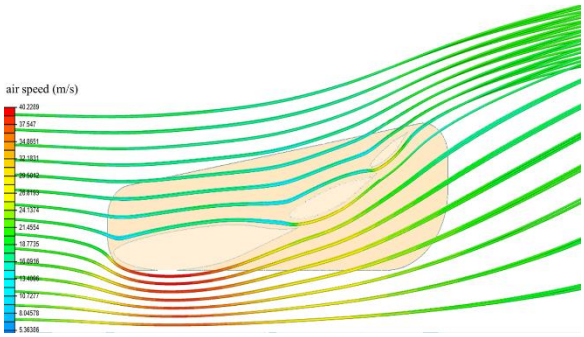

Figure 9. Obtained values of downforce for configuration 3 (Krušvar, 2024)

3.1.5 Configuration 7

Configuration 7 was selected for detailed full-vehicle simulations because it provided the most favourable balance between aerodynamic loading, flow behaviour and integration capability. Although Configuration 2 generated the highest downforce values (213.8 N), it exhibited flow separation on the second flap, reducing its suitability for practical implementation. The modified variants successfully eliminated separation but also reduced aerodynamic loading. Configuration 3 achieved the highest aerodynamic efficiency based on the lift-to-drag ratio (L/D = 17.07), although it generated lower downforce values compared to other concepts.

Configuration 7, consisting of an Eppler 664 main wing, MSHD first flap, and S1223 second flap, provided a compromise between downforce generation (190.14 N), aerodynamic stability and manufacturability. Configuration 7 geometry enabled successful integration with the complete vehicle and additional aerodynamic optimization around the diffuser region. To improve airflow control around the vehicle, an additional plate was installed parallel to the inner tire surface to redirect airflow toward the diffuser. Five modified variants (7 mod 1–7 mod 5) were analysed by varying the element positions and relative angles. Although these modifications reduced downforce values (132.83–139.08 N), they also reduced drag and improved flow quality around the vehicle, indicating improved aerodynamic efficiency during full-car simulations, Figures 10-11.

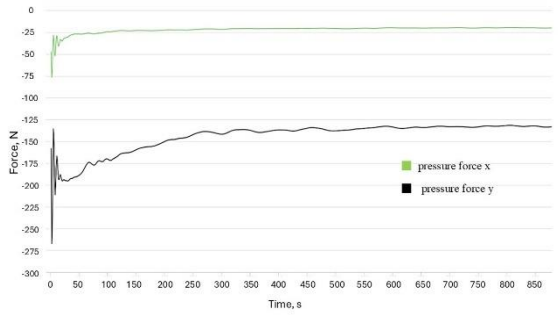

Figure 10. Resulting downforce for configuration 7 (Krušvar, 2024)

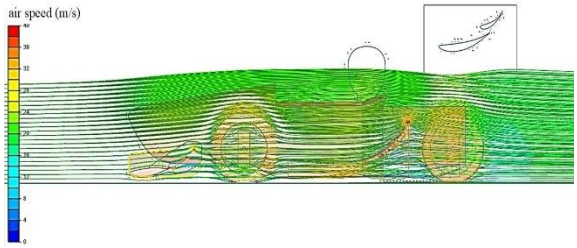

Figure 11. View of airflow profile simulation for the entire racing car (Krušvar, 2024)

3.2 Mold design

A smooth spoiler surface was created using negative moulds developed with the Mold Design tool in SolidWorks. Each part needed an upper and a lower mould half. To simplify the manufacturing process, the moulds for smaller parts were combined into one unit, as shown in Figure 12.

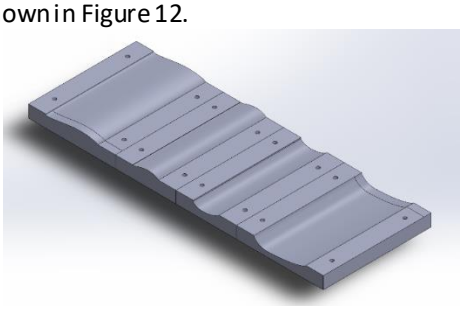

Figure 12. Profile fabrication molds (Krušvar, 2024)

To attach the spoiler to the chassis, it was necessary to construct sleeves onto which the spoiler would be connected. The sleeves were welded to the chassis at the designated locations. To facilitate the assembly of the spoiler and increase precision, templates were made for positioning the spoiler elements during assembly. These templates were attached to the boards and aligned with their edges. The slots on them served as guides for positioning the spoiler elements, Figure 13. The boards were cut using water jet process.

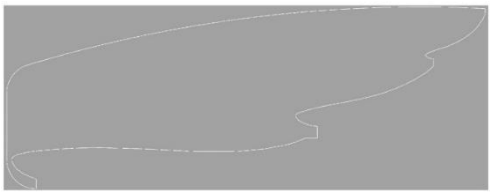

Figure 13. Templates for assembling (Krušvar, 2024)

To prevent spoiler breakage upon ground impact due to braking or passing over a hole, reinforcements that come with the plates were installed in the main wing. A total of 8 aluminium reinforcements, each 5 mm thick, were installed. After receiving the molds from the factory, they first had to be sanded to correct

the irregularities caused by cutting. Smaller parts of the mold were produced using 3D printing with Polylactic Acid (PLA) material, while larger pieces were made using Styrofoam. All irregularities were corrected with putty so that the most ideal shape possible could be obtained. Filling and sanding were repeated until the desired surface quality was achieved, onto which several coats of spray filler were later applied. The spray filler was sanded using sandpaper with grits of 600, 800, and 1200, and finally, everything was polished with polishing paste.

After the molds were made, the production of carbon profiles began. The profiles were made from an upper and lower part, which are bonded with resin after lamination into one piece. The technique used for making components was vacuum resin infusion. The molds were coated with a special liquid to facilitate the release of the profiles from the molds (the coating process was repeated at least four times). After cutting and placing two layers of carbon, a 2 mm Lantor Soric core was added, followed by another two layers of carbon, Figure 14. Unidirectional carbon fiber was used in the front spoiler, which transfers force along a specific axis. The lamination can be seen in the image below, along with how the vacuum draws the resin onto the necessary surface. The resin was mixed with a hardener in a 1:27 ratio and has about two hours before it starts to cure. Full curing requires a minimum of 24 hours. After this period, the vacuum bag can be removed and the profile separated from the mold, Figure 15.

Figure 14. Two layers of carbon and core before laminating (Krušvar, 2024)

Figure 15. Vacuum infusion process (Krušvar, 2024)

After the profiles dried, it was necessary to assemble both profiles into one. The spoiler was assembled by placing 8 aluminium reinforcements inside, which were cut with a 5mm water jet. The ends were connected with 20mm diameter carbon tubes to prevent the spoiler from bending at higher speeds, Figure 16.

Figure 16. Assembly and reinforcement of the front spoiler (Krušvar, 2024)

After the resin hardened for 24 hours, all surface irregularities were sanded. The sanding was conducted in several stages, using sandpaper with different grits: 180, 600, 900, and 1200. Once satisfactory surface quality was achieved, the spoiler was repainted. The goal was to create a final matt finish and add mechanical protection, as shown in Figure 17. To evaluate compliance with lightweight design requirements, the measured mass of the manufactured spoiler was compared with the target design value defined during the development phase. This comparison enabled assessment of the influence of the manufacturing process, resin uptake and reinforcement implementation on the final component weight. The obtained results confirmed whether the produced CFRP spoiler satisfied the intended lightweight design objectives while maintaining structural integrity and aerodynamic functionality.

Figure 17. Coating of the produced elements (Krušvar, 2024)

4 Conclusion

Recent studies continue to confirm the increasing role of CFRP materials in motorsport applications due to their favourable strength-to-weight ratio and manufacturing flexibility for aerodynamic components (Ahmad et al., 2020; Coşkun et al., 2025). Recent investigations have also shown that aerodynamic optimization using CFD tools significantly improves race car performance and enables early validation of spoiler designs before manufacturing (Gilchrist and Curley, 1999; Ozkan, Gok

and Karaoglanli, 2020). This paper contributes to the field of CFRP applications in building racing vehicle parts. It provides a clear overview of the manufacturing process and highlights the key testing phases needed before installation in a vehicle. Based on the research and practical work done, CFRP materials show important benefits in motorsport applications. They combine high strength with low weight, resist corrosion, and can be shaped accurately, making them ideal for high-performance use. The paper details the production steps, including vacuum resin infusion and the use of precision molds, which help create high-quality CFRP components.

The study further demonstrates how experimental validation and numerical simulations can be combined to verify structural and functional performance prior to vehicle integration. The proposed front racing car spoiler serves as an example, where careful planning and testing of CFRP components resulted in a notable improvement in aerodynamic performance and vehicle stability at high speeds.

In conclusion, this work not only confirms the advantages of CFRP composites in racing applications but also provides a step-by-step guide for their production and testing. It serves as a helpful reference for engineers, designers, and researchers working on lightweight, durable, and aerodynamically optimized components in the modern automotive industry. Finally, this paper provides a valuable contribution for educators seeking subjects that incorporate real-world engineering projects into technology and materials engineering curricula.

References

Ahmad, H., Markina, A.A., Porotnikov, M.V., Ahmad, F. (2020). A review of carbon fiber materials in automotive industry. *InIOP Conference Series: Materials Science and Engineering*, *971*(3), 032011). IOP Publishing.

Airfoil Tools (2025). Airfoil database [Internet]. [cited 2025 Jun 5]. Available from: http://airfoiltools.com/

Coşkun, A., et al. (2025). 'Investigation of the Effect of the Cutting Parameters on Cutting Forces and Tool Wear in the Stack Drilling of a Carbon Fibre-Reinforced Thermoplastic Matrix Composite and AA7075'. *Transactions of FAMENA*, *49*(1), 69-86.

Deakin, A. and Crolla, D. (2000). Fundamental Parameter Design Issues Which Determine Race Car Performance. *Motorsports Engineering Conference & Exposition*, Dearborn, Michigan, United States, November 13. doi: 10.4271/2000-01-3537.

Gilchrist, M.D. and Curley L. (1999). Manufacturing and ultimate mechanical performance of carbon fibre-reinforced epoxy composite suspension push-rods for a Formula 1 racing car. *Fatigue & fracture of Engineering materials & structures*, *22*(1), 25-32.

Krušvar, M. (2024). The use of carbon fiber reinforced composites in the production of racing vehicle components. Thesis. University of Rijeka. https://urn.nsk.hr/urn:nbn:hr:231:905531 (Accessed: 5 June 2025).

Ma, X. (2024). Numerical Simulation of Flow Over a Car and the Effects of Rear Airfoil-Shaped Spoiler. *InASME International Mechanical Engineering Congress and Exposition 2024*, Nov 17 (Vol. 88667, p. V008T10A005). American Society of Mechanical Engineers.

Ozkan, D., Gok, M.S., Karaoglanli, A.C. (2020). Carbon fiber reinforced polymer (CFRP) composite materials, their characteristic properties, industrial application areas and their machinability. *Engineering Design Applications III: Structures, Materials and Processes*, 235-53. doi: 10.1007/978-3-030-39062-4_20

Rehkopf, J.D. (2011). Automotive carbon fiber composites. SAE International; 2011 Nov 29.

Roslan, M.H., Hasbullah, H.H., Ramesh, T., Didane, D.H., Manshoor, B., Kabrein, H.A. (2023). Effect of a Spoiler on the Aerodynamic Performance of a Race Car on Track Using Two Different Turbulence Models. *Journal of Design for Sustainable Environment*, *5*(2), 28-37.

Savage G. (2008). Composite materials technology in formula 1 motor racing. Honda Racing F1 Team. 1, 109-39.